Journal of Membrane Science 659 (2022) 120775

Contents lists available at ScienceDirect

Journal of Membrane Science

journal homepage: www.elsevier.com/locate/memsci

Ultra-stable copper decorated deep eutectic solvent based supported liquid membranes for olefin/paraffin separation: In-depth study of carrier stability

Mi Xu, Haozhen Dou, Feifei Peng, Na Yang, Xiaoming Xiao, Xiaowei Tantai, Yongli Sun, Bin Jiang, Luhong Zhang *

School of Chemical Engineering and Technology, Tianjin University, Tianjin, 300072, China

ARTICLE INFO

Keywords:
Carrier stability
Deep eutectic solvents
Olefin/paraffin separation
Membrane separation
Carrier-facilitated transport

ABSTRACT

Great efforts have been made to develop versatile membranes with carrier-facilitated transport mechanism for olefin/paraffin separation. However, carrier instability has been an overwhelming roadblock, and manufacturing stable membranes have not yet been fulfilled, especially for copper salt-based membranes. Herein, a family of innovative deep eutectic solvents (DESs) were designed by utilizing Brønsted-acidic ammonium salts as hydrogen bond acceptors, which can stabilize CuCl carrier efficaciously. Then, stable copper-decorated deep eutectic solvent based supported liquid membranes (Cu-DESMs) were constructed by confining the as-designed DES and CuCl into porous support for the effective ethylene/ethane separation, where the morphology, molecular interactions and the structure-performance were revealed. The Cu-DESMs exhibited high ethylene permeability of 32.7 Barrer and ethylene/ethane selectivity of 26.8, which far exceeded most of copper salt-based membranes. Particularly, the Cu-DESMs exhibited long-term stability, and the investigation of carrier stability mechanism revealed that deactivation of copper salt-based carriers was included by disproportionation or oxidation reactions, and strong hydrogen-bond interactions and encapsulation effect favored carrier stability. This work offers preliminary guidance for designing stable carrier, and the ultra-stable Cu-DESMs with Brønsted-acidic property will make membrane separation move a step toward practical ethylene/ethane separation.

1. Introduction

Olefins, are the essential feedstocks to produce commonly used plastics and chemicals, and the separation of olefin/paraffin mixtures is critical in the petrochemical industry [1]. Cryogenic distillation is the most reliable technology to perform the olefin/paraffin separation, but requires huge capital and operating costs, which have created enough incentives to develop energy-effective and sustainable alternatives for the olefin/paraffin separation. Over the past thirty years, membrane technology has evolved as a promising approach for olefin/paraffin separation [2,3]. Versatile membranes with novel materials and structures have been developed such as polymer membranes [4,5], mixed matrix membranes (MMMs) [6–10], carbon molecular sieve (CMS) membranes [11,12], zeolite membranes [13], metal organic framework (MOF) membranes [6,14], and carrier-facilitated transport membranes (FTMs) [1,15,16]. Compared with membranes with solution-diffusion mechanism or molecular sieving mechanism, membranes with carrier-facilitated transport mechanism naturally possess high permeability and olefin/paraffin selectivity. Olefin molecules are transported initiatively via the carrier, and the separation performance of FTMs can be further improved by the rational design of membrane matrix and carrier [1,16–18]. FTMs are constantly developing and booming with the emergence of novel materials, where 2D nanosheets [19–21], MOF [22–24], ionic liquids (ILs) [25–29], and deep eutectic solvents (DESs) [30,31] have been utilized as membrane materials for the construction of advanced FTMs.

Despite the intensive research, the carrier chemical stability of FTMs is still a daunting challenge, which has been ignored in the multitude of previously published papers [32–34]. Currently, the widely used carriers for olefin/paraffin separation can be divided into two categories: copper(I)-based carriers and silver-based carriers, including metal salts (such as $AgBF_4$, $AgNO_3$, and CuCl) or metal nanoparticles. The carrier is dispersed into the membrane matrix to generate metal ions (Ag^+ and Cu^+), metal complex ions ($CuCl_2^-$), or positively-charged nanoparticles via the interactions with membrane matrix, thus significantly accelerating the transport of olefin molecules. Among them, the

* Corresponding author.
E-mail address: zhanglvh@tju.edu.cn (L. Zhang).

https://doi.org/10.1016/j.memsci.2022.120775
Received 1 March 2022; Received in revised form 8 May 2022; Accepted 22 June 2022
Available online 24 June 2022
0376-7388/© 2022 Elsevier B.V. All rights reserved.

positively-charged copper or silver nanoparticles exhibit good stability but low olefin/paraffin selectivity, and special electron acceptors are needed to activate the surface charge of nanoparticles [35,36]. Silver salts possess the best ability to transport olefin molecules, which render the resultant membranes with extremely high olefin/paraffin selectivity. Meanwhile, several effective strategies have been proposed to stabilize silver salt, including the introduction of $Al(NO_3)_3$ and Ag_2O [37], adopting protic ILs as membrane matrix [38–40], as well as developing regeneration method that uses a peroxide/acid liquid or vapor phase treatment to oxidize the reduced silver carriers [32]. Copper salts have the attributes of low-cost, facile availability and satisfactory olefin/paraffin selectivity. Jiang et al. utilized DESs as membrane matrix to dissolve CuCl carrier for the ethylene/ethane separation [15,30]. Then, Sun et al. fabricated copper(I)-based IL membranes with carrier-facilitated transport mechanism for ethylene/ethane separation, and the carrier activity can be improved by adding other metal salt such as $ZnCl_2$ [41,42]. Although the great potential of membranes containing copper salt as carrier has been demonstrated, the development of membranes with copper salt as carrier are seriously lagging compared with those based on silver salt, and only few research pays attention to carrier stability and the development of effective strategy for the enhanced carrier stability.

In this work, a family of innovative DESs were designed by adopting protonated ammonium salts as hydrogen bond acceptors (HBAs) and polyol as hydrogen bond donors (HBDs), which rendered the DESs with Brønsted-acidity, thus affording long-term carrier chemical stability. DESs were voted as membrane matrix due to their distinct advantages of low-cost, synthetical accessibility, structural flexibility, facile fabrication of defect-free membrane, and higher gas permeability in relative to solid membranes due to the faster gas diffusion in liquid than solid [43–47]. Then, a series of copper-decorated DES based supported liquid membranes (Cu-DESMs) with carrier-facilitated transport mechanism were constructed by confining as-designed DES and CuCl carrier into porous support for ethylene/ethane separation. By the virtue of rational design of DESs, the Cu-DESMs exhibited high ethylene permeability and ethylene/ethane selectivity, which exceeded the-state-of-the-art membranes. Particularly, the Cu-DESMs possessed long-term stability, which was highlighted by comparing with the most prevailing FTMs utilizing IL or DES as membrane matrix and CuCl as carrier, revealing the deactivation mechanism of copper salt-based carriers as well as offering guidance for realizing carrier stability.

2. Experimental

2.1. Materials

Ethylamine (>98.0%), diethylamine (>98.0%), triethylamine (>99.0%), ethanolamine (>98.0%), diethanolamine (>98.0%) and hydrochloric acid (HCl, 37.0%) were bought from Shanghai D&B Biological Technology Co., Ltd. Ethylene glycol (EG, >99.0%), diethylene glycol (DEG, >99.0%) and glycerol (G, 99.5%) were supplied from Heowns Biochem Technologies. LLC. 1-Butyl-3-methylimidazolium chloride ([Bmim][Cl]) (≥99.5%) was offered by Lanzhou Institute of Chemical Physics, Chinese Academy of Sciences. Copper(I) chloride (CuCl, AR, 97.0%) was obtained from Macklin Biochemical Co., Ltd and recrystallized by HCl prior to use. Nylon support membranes (pore size of 0.1 μm, porosity of 75%, average thickness of 100 μm, diameter of 75 mm) were kindly provided by Haining Zhongli Filtering Equipment Corporation (China). Ethylene (C_2H_4, >99.5%), ethane (C_2H_6, >99.5%) and nitrogen gas (N_2, 5 N) were purchased from Air liquid Holding CO., LTD.

2.2. Preparation of Cu-DESMs

The fabrication of Cu-DESMs comprised four steps: synthesis of protonated HBAs via proton-transfer reaction; preparation of DESs via simple mixing of HBA and HBD at the desired molar ratio; dissolution of CuCl carrier in DESs to get homogeneous membrane liquid containing copper complex anions as reactive carrier; fabrication of Cu-DESMs via pressure-assisted filtration method (Fig. 1a). The chemical structures of HBAs and HBDs are shown in Fig. 1b, and structure of Cu-DESM is shown in Fig. 1c.

Four different protonated ammonium salts of ethylamine hydrochloride (EAHCl), diethylamine hydrochloride (DEAHCl), ethanolamine hydrochloride (EoAHCl) and diethanolamine hydrochloride (DEoAHCl), acting as HBAs, were synthesized by proton-transfer reaction between amine and HCl according to previous procedure with slight modifications [40]. Then, DES was synthesized by simply mixing HBA and HBD (including EG, DEG and G) by heating at 60 °C under magnetic stirring for 8 h until a colorless and homogeneous liquid was formed. The copper-decorated DES (Cu-DES) was prepared through dissolving the as-purified CuCl into DES by heating at 70 °C for 2 h under vigorous stirring, followed by degassing in a vacuum oven for 4 h. After that, Cu-DESMs were prepared by confining Cu-DES into porous Nylon support via the pressure-assisted filtration method [31]. The Nylon support was firstly placed in a vacuum oven for 4 h to remove residual gas in the pores, and Cu-DES was uniformly spread onto the top surface of support with a dropper. Subsequently, the membrane was transferred into a permeation cell, and the Cu-DES was pressed into the membrane pores under the pressure of 1 bar. This procedure was repeated for three times until a thin layer of green liquid appeared on the bottom of support, which indicated the membrane pores were filled with Cu-DES. Eventually, Cu-DESMs were obtained by carefully wiping the excess liquid on the membrane surface with tissue. Control membranes without CuCl carrier were also prepared using the above-described procedure. The loading amount of the Cu-DES in the membrane was calculated by the following equation: $m = m_1 - m_0$, where m_0 and m_1 were the mass of the Nylon support before and after the injection of Cu-DES. When the CuCl/[EAHCl][G] mixed solution (molar ratio of HBA and HBD at 1:2 and CuCl concentration at 3 mol/L) was used, the loading amount was 346.5 mg. For investigation of carrier stability, two previously reported membranes in literature were also fabricated, where DES-FTMs were prepared with DES utilizing [Bmim][Cl] acts as HBA and G acts as HBD (the molar ratio of [Bmim][Cl] to G at 1:2 and CuCl concentration at 3 mol/L), and the IL-FTMs were prepared by CuCl-containing IL based on [Bmim][Cl] and CuCl (the molar ratio of [Bmim][Cl] to CuCl at 1:2). The fabrication procedure was similar with that of Cu-DESMs except for the liquid used.

2.3. Characterization

^{1}H nuclear magnetic resonance (^{1}H NMR) spectra were recorded by VARIA INOVA 500 MHz spectrometer with deuterated dimethyl sulfoxide (DMSO-d_6) as solvent and tetramethyl silane (TMS) as the external reference. Attenuated total reflection Fourier transform infrared spectra (ATR-FTIR) were collected on a Bio-Rad FTS 6000 FTIR spectrometer with 32 scans covering a range of 500–4000 cm^{-1}. X-ray diffraction (XRD) patterns were conducted by using X'Pert Pro X-ray diffractometer with a Cu Kα radiation (λ = 1.5418 Å) under a potential of 40 kV and an applied current of 40 mA, which was performed from 5° to 90° with a step size of 0.1°. Deep eutectic points were obtained by a TA Q2000 differential scanning calorimeter (DSC) according to the following procedure: the sample (5–10 mg) was enclosed in sealed aluminum pans and experienced cooling from room temperature to −150 °C, and then heating from −150 °C to 100 °C under a continuous flow of dry nitrogen with the heating/cooling rate setting at 10 °C/min. Thermal stability was determined by a NETZSCH TG 209 thermal gravimetric analyzer in the temperature range of 20–690 °C in nitrogen atmosphere with a healing rate of 10 °C/min. The morphology was observed by Hitachi S-4800 Field-emission scanning electron microscopy (SEM) equipped with energy dispersive spectrometry (EDS).

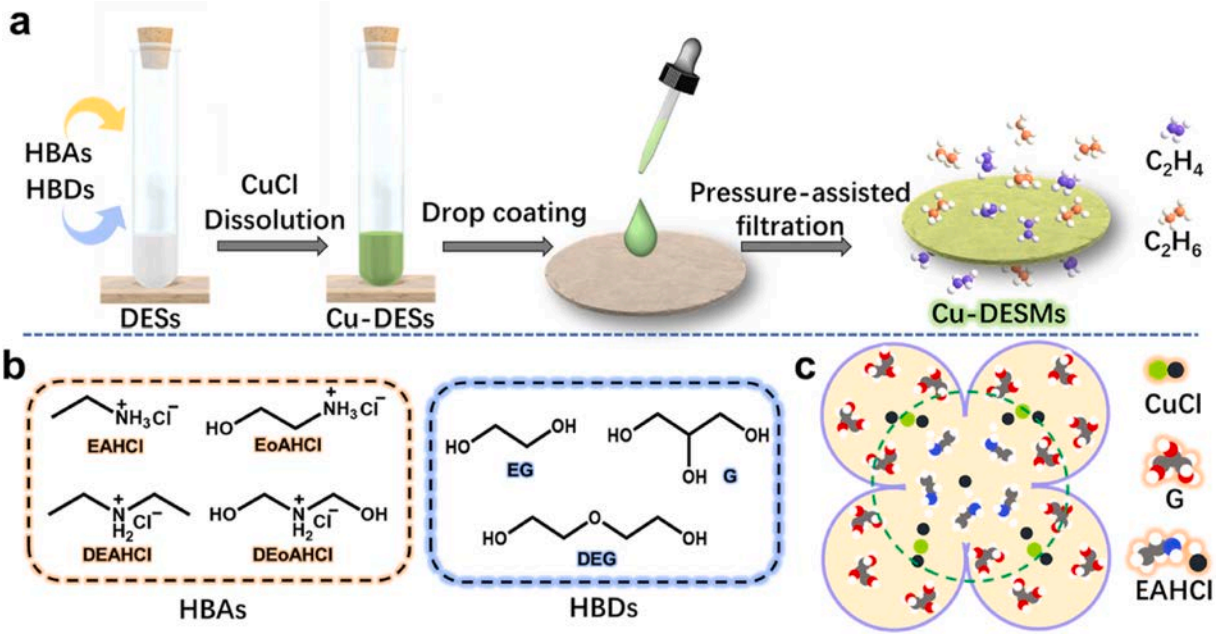

Fig. 1. (a) Fabrication of Cu-DESMs. (b) Chemical structures of HBAs and HBDs. (c) The structure of Cu-DESM, where EAHCl acting as HBA and G acting as HBD.

2.4. Separation performances

The separation performances of Cu-DESMs were measured by a custom-made apparatus (Fig. S1) according to the below procedure. A freshly prepared Cu-DESMs was fixed in a stainless-steel permeation cell with a feed compartment and a permeate compartment, which was placed inside an air blowing thermostatic oven for easily adjusting temperature. And, the pressure of the feed compartment was adjusted by a needle valve and the pressure value was recognized by a pressure transducer with an accuracy of 0.001 bar. Before measuring gas permeability, air tightness inspection of the apparatus was conducted by filling with nitrogen at pressure of 2 bar and good air tightness was established by the maintenance of constant pressure for 1 h. Then, pure C_2H_4 and C_2H_6 with a flow rate of 30 mL/min (STP) were introduced into a static mixer to get equimolar mixed gas, and the mixed gas entered the feed compartment and reached the permeate compartment at 0.1 bar through the Cu-DESMs to achieve effective separation. Meanwhile, the nitrogen with a flow rate of 20 mL/min (STP) was used as sweeping gas and the flow rate was precisely controlled by a mass flow controller with an accuracy of ±0.5% and the gas composition was monitored by an online gas chromatography system (Model GC 2008B, Lunan, equipped with a gas autosampler and a flame ionization detection device) every 10 min.

The C_2H_4 permeability or C_2H_6 permeability through the membrane was calculated according to formula:

$$P_i = J_i \times \frac{\delta}{\Delta P_i} = \frac{V_{STP,i}}{A} \times \frac{\delta}{\Delta P_i} \quad (1)$$

where J_i is the permeation flux of the component *i*, cm^3/cm^2s; δ is the membrane thickness, the value is 100 μm; ΔP_i is the partial pressure of the component *i* through the membrane, bar; $V_{STP,i}$ is the volume flow of the component *i* at standard conditions, cm^3/s (STP); A is the effective area of the membrane, 19.625 cm^2 is used in this paper. The gas permeability is expressed in Barrer, 1 Barrer = 10^{-10} (cm^3 (STP) cm)/(cm^2 cmHg s).

The C_2H_4/C_2H_6 separation selectivity was defined as the ratio of C_2H_4 permeability to C_2H_6 permeability:

$$S = \frac{P_{C2H4}}{P_{C2H6}} \quad (2)$$

The gas solubility and diffusivity in Cu-DESMs were determined according to the method described in our previous publication [38], and the detailed process was presented in Supporting Information.

3. Results and discussion

3.1. Chemical structure of Cu-DESMs

The chemical structures of the DESs and Cu-DESs were investigated by ^{1}H NMR and ATR-FTIR spectroscopy, which revealed the formation mechanism of DESs as well as mechanisms of carrier activity and stability. ^{1}H NMR spectra of three DESs at different HBA-HBD molar ratios showed characteristic peaks of both EAHCl and G, which confirmed the successful synthesis of DESs (Fig. 2a). For example, ^{1}H NMR spectrum of DES at molar ratio 1:1 showed chemical shifts at 8.026 ppm (-NH_3^+ of EAHCl), 4.601 ppm (-OH of G), 3.304 ppm (-CH/CH_2 of G), 2.823 ppm (-CH_2 of EAHCl) and 1.176 ppm (-CH_3 of EAHCl). The chemical shift of –NH_3^+ exhibited the weakened intensity upon mixing with G, and decreased significantly from 8.197 ppm to 8.026 ppm, 7.970 ppm, and 7.893 ppm for the molar ratios of EAHCl to G at 1:1, 1:2 and 1:3, respectively, indicating that G molecule inserted into the EAHCl and broke the electrostatic interaction between anions and cations. Besides, the –OH chemical shift of G also became weak and broad, and shifted to down-field from 4.451 ppm to 4.601 ppm, 4.547 ppm and 4.524 ppm for the molar ratio of 1:1, 1:2 and 1:3, respectively, which suggested the newly-formed hydrogen-bond interactions between G and EAHCl. The intermolecular interactions between HBA and HBD were further confirmed by ATR-FTIR spectra (Fig. 2b). In the spectrum of DES at molar ratio of 1:1, the peak at 3295 cm^{-1} was the characteristic peak of the –OH stretching vibration, the peaks at 2066 cm^{-1} and 1505 cm^{-1} were assigned to the symmetrical stretching vibration and deformation vibration of –NH_3^+, respectively, and the characteristic peak at 1610 cm^{-1} corresponded to the bending vibration of –NH_2 [48]. With the molar ratio of EAHCl to G varying from 1:1 to 1:3, the peaks of –OH stretching exhibited red-shift while the peaks associated with the amino groups exhibited blue-shift, which illustrated the hydrogen-bond interactions were formed between G and Cl^- and the ordered structure of EAHCl was disrupted. The ^{1}H NMR and ATR-FTIR spectra of DESs with different HBA-HBD combinations (Fig. S2) exhibited similar behaviors with [EAHCl][G] based DES, which has been detailed in the Supporting

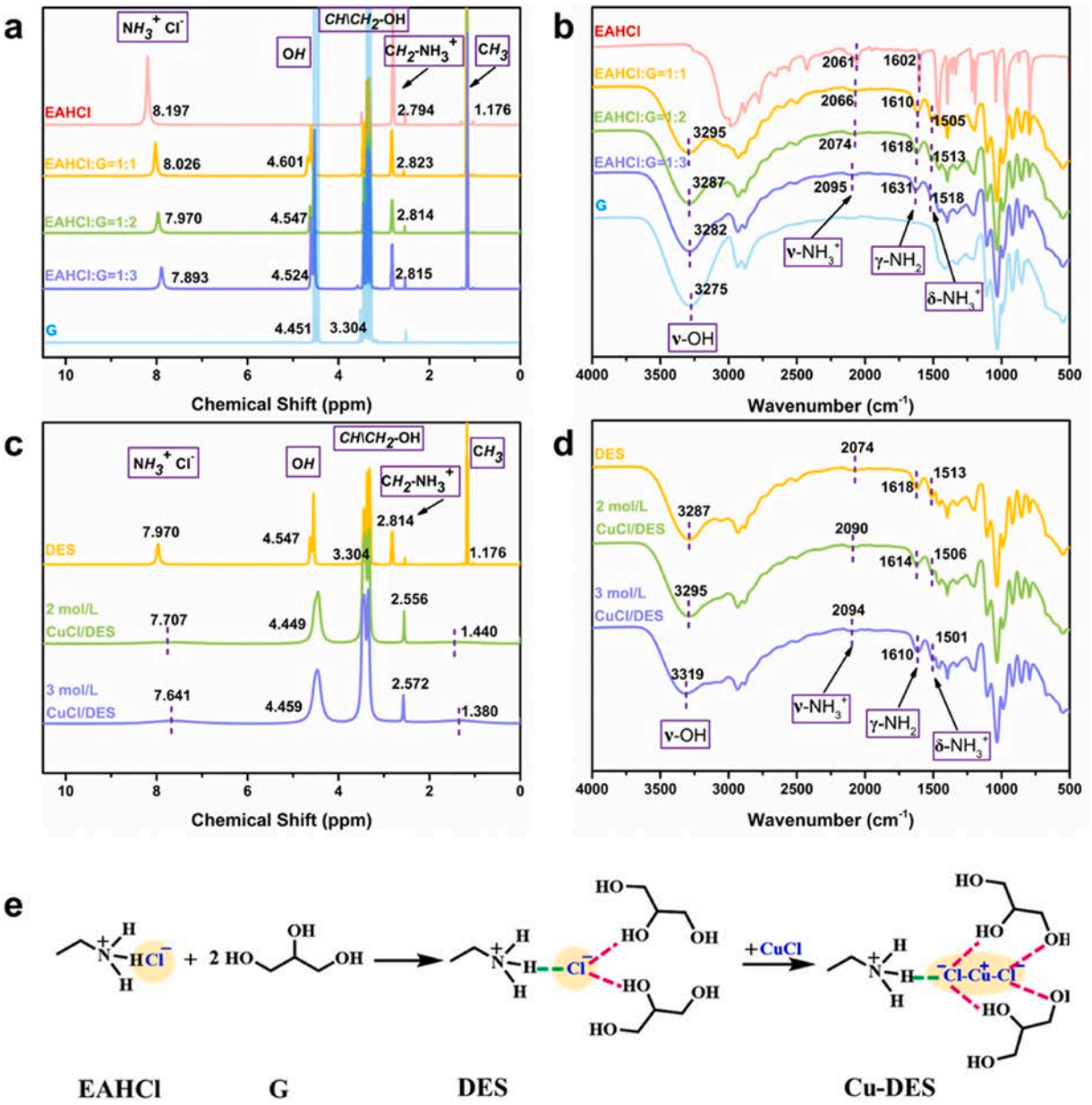

Fig. 2. Structure and chemistry of Cu-DESMs. (a, b) Investigation of intermolecular interactions deriving the formation of DESs by ^{1}H NMR and ATR-FTIR spectra, where [EAHCl][G] based DESs with different molar ratios act as examples. (c, d) Investigation of intermolecular interactions within Cu-DESMs by ^{1}H NMR and ATR-FTIR spectra to reveal the mechanism of carrier activity and carrier stability, where the [EAHCl][G] based DES with the molar ratio of HBA and HBD at 1:2 is used. (e) Complexation reaction between CuCl and Cl^- to generate $[Cu_xCl_y]^{z-}$ anions.

Information. Obviously, the extent of peak varies with different DES structures, which means the intensity of the interactions within DES can be tuned by the appropriate selection of HBAs and HBDs. The above results confirmed the formation mechanism of DESs that the weakened electrostatic interactions between anion and cation as well as newly formed hydrogen-bond networks between HBA and HBD for charge delocalization accounted for the formation of stable liquid.

^{1}H NMR and ATR-FTIR spectra of Cu-DESMs provided more information about molecular interactions between CuCl and DESs (Fig. 2c–d and Fig. S3). After the dissolution of the CuCl in the DESs, the chemical shift of $-NH_3^+$ decreased from 7.970 ppm to 7.707 ppm and then to 7.641 ppm at carrier concentrations of 2 mol/L and 3 mol/L, accompanying with the significantly weakened peak intensity (Fig. 2c). Meanwhile, $-CH_3$ (EAHCl) also had a broader but significantly weakened peak with the addition of CuCl carrier. The dramatic variation in chemical shift and peak intensity of EAHCl was attributed to the complexation reaction between CuCl and Cl^- to generate $[Cu_xCl_y]^{z-}$ anions as well as the strong hydrogen-bond interactions between $[Cu_xCl_y]^{z-}$ and proton of $-NH_3^+$ (Fig. 2e and Fig. S4). As for G, the sharp splitting peaks of –OH evolved into a broad peak and the corresponding chemical shift of –OH moved to up-field and then to down-field with the increase of CuCl concentration, which was due to the destruction of hydrogen-bond interactions between G and G and the re-construction of hydrogen-bond interactions between G and $[Cu_xCl_y]^{z-}$ anions. The newly formed hydrogen-bond interactions meant the complete solvation of $[Cu_xCl_y]^{z-}$ anion carriers and rendered the carrier with encapsulation effect. As further indicated by ATR-FTIR spectra, the –OH stretching vibration peak exhibited blue-shifts after the addition of CuCl, indicating the weakened hydrogen-bond interactions of G-G. With the increase of carrier concentration, the characteristic peak of symmetrical stretching vibration of $-NH_3^+$ increased continuously from 2074 cm^{-1} to 2094 cm^{-1}, while that of bending vibration of $-NH_2$ decreased from

1618 cm^{-1} to 1610 cm^{-1}, respectively, which demonstrated that the strong hydrogen-bond interactions between the $–NH_3^+$ and carriers favored the proton transfer from $–NH_3^+$ to carriers, inducing slightly deprotonation of $–NH_3^+$ to $–NH_2$ group. Therefore, the adoption of DESs with Brønsted-acidity created strong hydrogen-bond interactions between protonated cation and $[Cu_xCl_y]^{z-}$ anions.

The thermal properties of Cu-DESMs were also probed by DSC and TG characterizations. DSC curves displayed typical eutectic points of DESs between −100 °C and −80 °C, and the eutectic point increased with the decrease of molar ratio of HBA to HBD (Fig. 3a and Fig. S5). After the addition of carrier, the eutectic point of Cu-DES increased up to −79.36 °C and was still much lower than the melting points of the parent HBA and HBD, which suggested the Cu-DES still maintained the DES characteristics and the as-designed DESs were robust to achieve high carrier concentration. Moreover, the thermal decomposition temperatures of the DESs and Cu-DES were higher than 200 °C (Fig. 3b), confirming the satisfactory thermal stability. In addition, the Cu-DES showed a two-stage decomposition and the reduced rate of mass loss, demonstrating the enhanced thermal stability, which was favorable for gas separation in a large range of operating temperature.

3.2. Morphology of the Cu-DESMs

The morphology of Cu-DESM was investigated by SEM and EDS mapping. The optical image of Cu-DESM revealed a transparent and green membrane, which suggested the successful membrane fabrication (Fig. 4a). The surface image of Nylon support presented a hierarchical pore structure with pore size ranging from 100 nm to 1 μm (Fig. 4b). Regarding to Cu-DESM, the membrane pores were full of Cu-DES due to the positive capillary force and assistance of additional pressure (Fig. 4c). The cross-section images of Nylon support exhibited a typical sandwich configuration with a robust fiber middle layer between spongy top layer and bottom layer, which provided sufficient mechanical support and abundant pores for accommodations of Cu-DES (Fig. 4d–f). As further confirmed by cross-section images of Cu-DESM (Fig. 4g–i), Cu-DES was penetrated and connected throughout the entire membrane, and no unfilled pore was observed, which suggested the extremely compatibility between Nylon support and Cu-DES. Moreover, the EDS mapping revealed the well-distribution of Cu, Cl, N, C and O elements (Fig. 4j), which indicated that the Cu-DESM was successfully prepared.

3.3. Structure-performance relationship of Cu-DESMs

The structure-performance relationship of Cu-DESMs was investigated, including the effect of HBA, effect of HBD, effect of CuCl concentration and effect of molar ratio of HBA to HBD. As shown in Fig. 5a, the as-designed Cu-DESMs exhibited high C_2H_4 permeability and C_2H_4/C_2H_6 selectivity due to the rational structure design of HBAs and providential HBA-HBD combinations. The [EAHCl][G] based Cu-DESM exhibited the highest C_2H_4/C_2H_6 selectivity of 26.8 and excellent C_2H_4 gas permeability of 32.7 Barrer, while the [DEAHCl][G] based Cu-DESM obtained a slightly higher C_2H_4 permeability of 36.5 Barrer and lower C_2H_4/C_2H_6 selectivity of 18.2, which was attributed to the different cation sizes of HBAs. Larger cation size of HBA meant weaker electrostatic interactions between cation and anion, which resulted in a looser membrane structure, thus accelerating gas diffusion to get higher gas permeability. Compared with [EAHCl][G] based Cu-DESM, the Cu-DESMs fabricated with EoAHCl and DEoAHCl exhibited reduced gas permeabilities and C_2H_4/C_2H_6 selectivity. With extra hydroxyl groups in the HBAs, the newly-formed hydrogen-bond interactions within membranes afforded more compact membrane structure with high viscosity of Cu-DESs, which blocked the diffusion of C_2H_4 and C_2H_6. The [DEoAHCl][G] based Cu-DESM possessed a lower gas permeability than [EoAHCl][G] based Cu-DESM, which suggested the enhanced hydrogen-bond interactions by more hydroxyl groups dominated compared with the weakened electrostatic interactions due to larger cation size. Fig. 5b demonstrated the great effect of HBDs on the separation performance of Cu-DESMs. The effect of HBDs on C_2H_4 permeability followed the order: EG > DEG > G, and for the C_2H_4/C_2H_6 selectivity, a different order was observed: G > EG > DEG. The C_2H_4 permeabilities of Cu-DESMs with EG and DEG as HBAs were 299.4 Barrer and 116.6 Barrer, which were almost 9.2 and 3.6 times of that of G based Cu-DESM. This can be explained that G possessed more hydroxyl groups and generated stronger hydrogen-bond interactions, which resulted in the increased viscosity of Cu-DES, thus impeding gas diffusion and obtaining low permeability. However, C_2H_4/C_2H_6 selectivities of EG and DEG based Cu-DESMs were only 14.8 and 9.3, and G based Cu-DESM obtained the highest C_2H_4/C_2H_6 selectivity of 26.8. Compared with Cu-DESM with EG or DEG as HBDs, stronger hydrogen-bond interactions between hydroxyl from G and Cl^- from CuCl in G based Cu-DESM can weaken the interactions between Cu^+ and Cl^-, which effectively increased the interactions between Cu^+ and C_2H_4 molecules.

As seen from Fig. 5c, the effect of CuCl concentration on separation performances of Cu-DESMs was also investigated and highlighted by comparing with the control DESM without CuCl carrier. The C_2H_4 permeability and C_2H_6 permeability of the DESM without carrier were 8.06 Barrer and 3.88 Barrer, respectively, and the corresponding C_2H_4/C_2H_6 selectivity was only 2. In contrast, at the CuCl concentration of 3

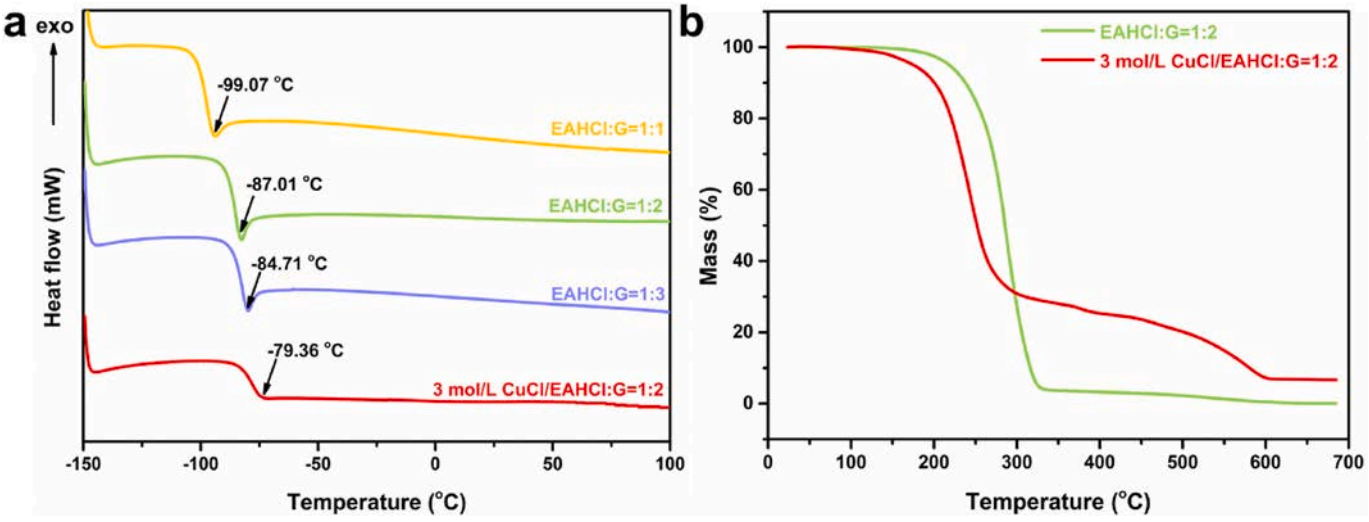

Fig. 3. The thermal properties of Cu-DESMs. (a) DSC and (b) TG curves of DES and Cu-DESMs.

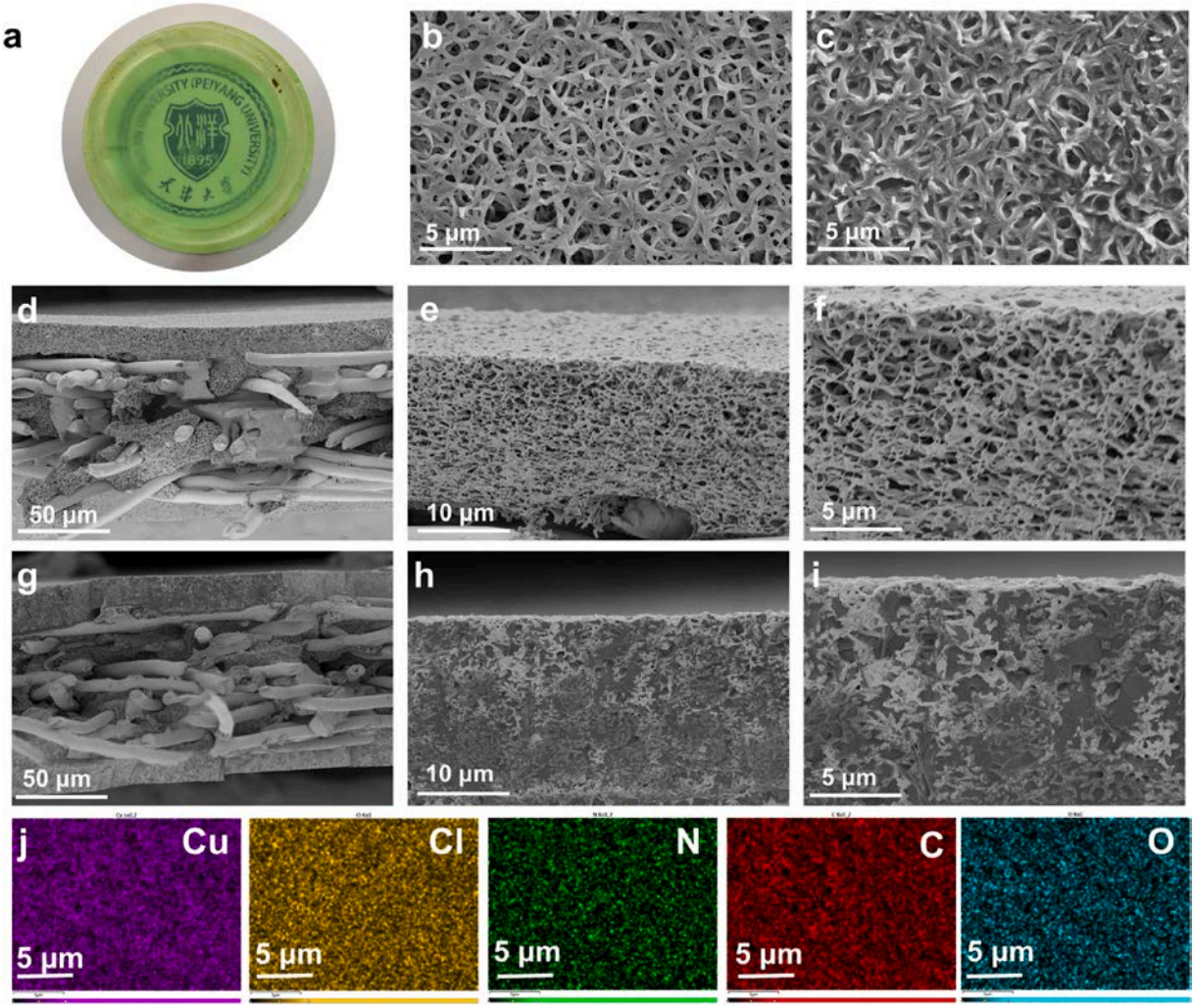

Fig. 4. The morphology of Cu-DESM, where [EAHCl][G] based DES has been used with the molar ratio of HBA and HBD at 1:2 and the concentration of CuCl at 3 mol/L. (a) Optical image of Cu-DESM. (b, c) Surface SEM images of Nylon support and Cu-DESM. (d, e, f) Cross-section SEM images of Nylon support and highlighting its spongy top layer at high-resolution. (g, h, i) Cross-section SEM images of Cu-DESM and highlighting the saturated pores with Cu-DES. (j) The corresponding EDS mapping of Cu-DESM collected from the surface of the Cu-DESM in Fig. 4c.

mol/L, the C_2H_4 permeability and C_2H_4/C_2H_6 selectivity of the Cu-DESM reached up to 32.7 Barrer and 26.8, respectively, which were much higher than those of DESM without carrier, confirming the carrier-facilitated transport mechanism. The drastic increase of C_2H_4/C_2H_6 selectivity further suggested the as-designed DESs were ideal solution for CuCl carrier to obtain high carrier activity. With the increase of CuCl concentration from 1 mol/L to 3 mol/L, the C_2H_4 permeability increased linearly, while the C_2H_6 permeability decreased remarkably. Based on the solution-diffusion theory [49,50], the permeability could further be represented as the product of thermodynamic solubility and kinetic effective diffusivity. With the increase of CuCl concentration, more carriers were available to coordinate with C_2H_4, while the solution of C_2H_6 was suppressed due to the salting-out effect, which leads to the sharp increase of the solubility selectivity. Both the C_2H_4 diffusivity and C_2H_6 diffusivity decreased with increasing CuCl concentration, thus the diffusivity selectivity decreased slightly due to the larger decrease of C_2H_4 diffusivity, which was probably due to the larger size of $[Cu_xCl_y(C_2H_4)_n]^+$ complex. Moreover, it can be clearly concluded that C_2H_4/C_2H_6 selectivity was dominated by the solubility selectivity (Table S1).

The molar ratio of HBA to HBD also regulated the separation performances of Cu-DESMs, which easily obtained the different combinations of C_2H_4 permeability and C_2H_4/C_2H_6 selectivity (Fig. 5d). As the molar ratio of HBA to HBD decreased from 1:1 to 1:3, the C_2H_4 and C_2H_6 permeabilities of the Cu-DESMs gradually decreased, but the C_2H_4/C_2H_6 selectivity increased significantly. For example, the C_2H_4 permeability and C_2H_4/C_2H_6 selectivity of Cu-DESM at molar ratio of 1:1 were 52.1 Barrer and 20, respectively. When the molar ratio reduced to 1:3, the C_2H_4 gas permeability dropped to 16.9 Barrer but the C_2H_4/C_2H_6 selectivity moderately elevated to 31.9. With the decrease of molar ratio, more G molecules were involved in membrane to create stronger hydrogen-bond interactions, which increased the viscosity of Cu-DES, thus reducing C_2H_4 and C_2H_6 permeabilities simultaneously. However, benefiting from carrier-facilitated transport mechanism, the decrease degree of C_2H_4 permeability was much lower than that of C_2H_6 permeability, which contributed to the significant increase of C_2H_4/C_2H_6 selectivity.

3.4. Optimization of operating conditions

Process optimization was also conducted to get effective separation. Accordingly, the effects of operating temperature and partial pressure on separation performances of Cu-DESMs were investigated. With the operating temperature increasing from 25 °C to 55 °C, opposite trends were observed in the gas permeability and separation selectivity (Fig. 6a). The C_2H_4 permeability increased from 32.7 Barrer to 53.7

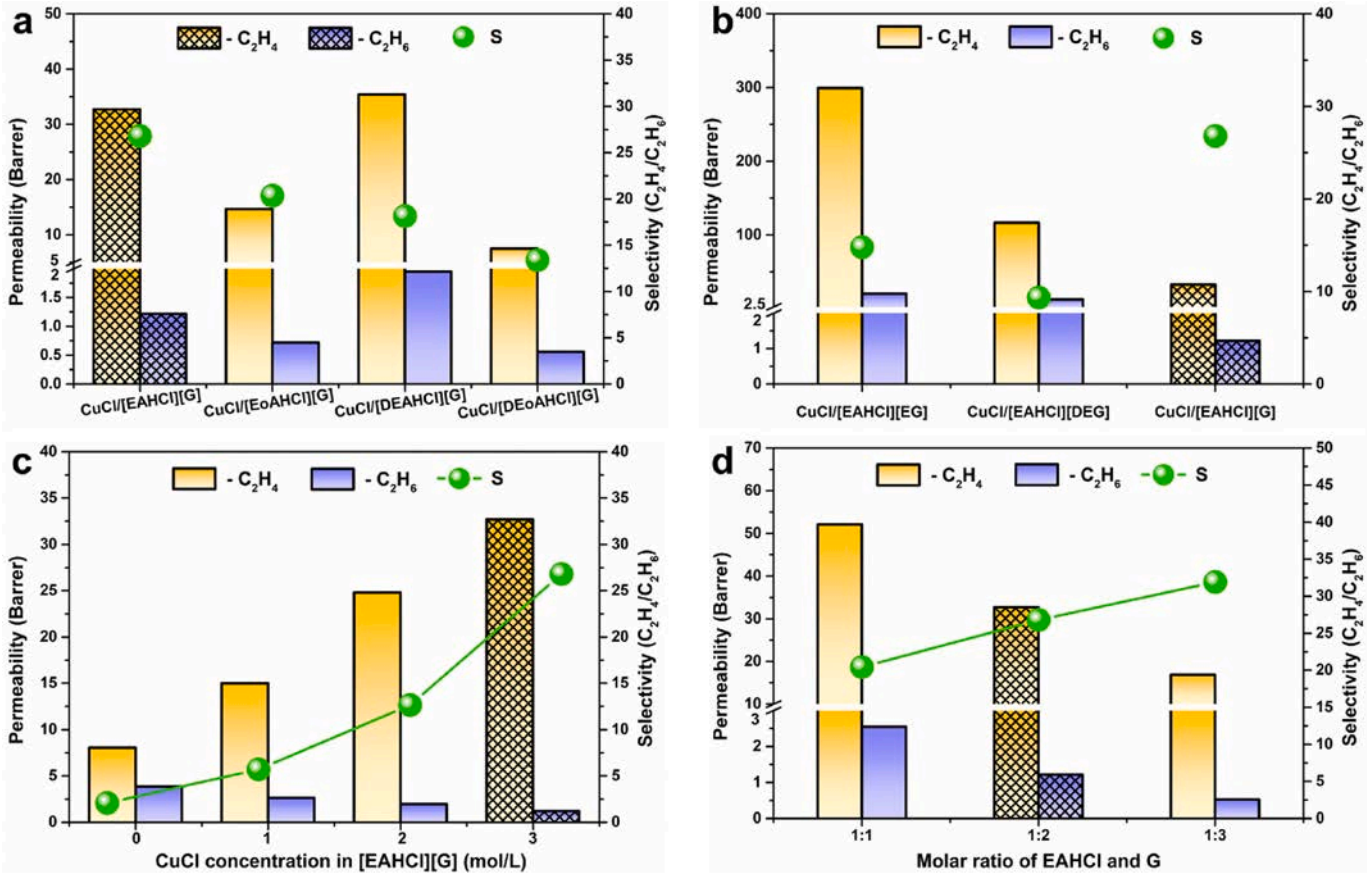

Fig. 5. Structure-performance relationship of Cu-DESMs. (a) Effect of the HBAs. (b) Effect of the HBDs. (c) Effect of the CuCl concentration. (d) Effect of the molar ratio of HBA to HBD. The test conditions: CuCl concentration of 3 mol/L, the molar ratio of HBA to HBD of 1:2, the pressure of 0.1 bar, the temperature of 25 °C and the gas flow rate of 60 mL/min (STP) with equal molar of C_2H_4 and C_2H_6 unless otherwise stated.

Barrer and the C_2H_6 permeability increased from 1.2 Barrer to 3.6 Barrer. The increase of operating temperature weakened the molecular interactions within membranes but enhanced the chain flexibility, which significantly enhanced the gas diffusion through the membranes, thus contributing to the increase of C_2H_6 and C_2H_4 permeability. However, the increase of C_2H_6 permeability was larger than that of C_2H_4 permeability, which was attributed to the negative effect of temperature on the carrier-facilitated transport mechanism. The increased temperature crippled the complexation between $[Cu_xCl_y]^{z-}$ anion carriers and C_2H_4, thus leading to the limited increase of C_2H_4 permeability. Therefore, the C_2H_4/C_2H_6 selectivity decreased from 26.8 to 15.1. As shown in Fig. 6b, as the partial pressure increased from 0.1 bar to 0.85 bar, the C_2H_4 permeability experienced a steady decrease from 32.7 Barrer to 13.1 Barrer, which was attributed to the limited carrier number. The carriers were easily saturated even at low pressure and failed to coordinate with C_2H_4 molecules at high pressure [38]. In contrast, the C_2H_6 permeability was almost unchanged with the increase of the partial pressure, which further confirmed the C_2H_6 permeation through Cu-DESMs was mainly dependent on solution-diffusion mechanism. Therefore, the C_2H_4/C_2H_6 selectivity reduced from 26.8 to 14.1. When the partial pressure increased to 1.0 bar, the gas permeability of C_2H_4 and C_2H_6 increased stupendously and the C_2H_4/C_2H_6 selectivity was 1.0, which indicated the membrane pores were punctured. The C_2H_4/C_2H_6 selectivity remained higher than 10 even under high temperature at 55 °C and partial pressure at 0.85 bar, which exhibited competitive operating stability of Cu-DESMs. Therefore, the ultimate pressure of Cu-DESMs reached up to 1.7 bar.

3.5. Stability of Cu-DESMs

Long-term stability was a crucial property for membrane separation. As revealed by Fig. 6c–d, both C_2H_4 and C_2H_6 permeabilities of Cu-DESMs experienced a decline in the first 2 h for separation due to the increased viscosity of Cu-DESs induced by the evaporation of absorbed moisture, and then leveled off with a slight fluctuation during the continuous 160-h operation. And the C_2H_4/C_2H_6 selectivity remained stable at around 27.0, which suggested the excellent stability of Cu-DESMs and great potential for long-time operation. However, it should be noted that the membrane was protected by the permeation cell and inert gases during permeation, which offered a dark and safe environment isolated from the oxygen and moisture.

The carrier stability was further investigated by placing the Cu-DESMs in a plastic-Petri-dish for two years without any protection. The Petri-dish has access to air and the Cu-DESMs contact with the oxygen, H_2O, and light. For comparison, the stability of prevailing DES or IL based carrier-facilitated transport membranes (DES-FTMs and IL-FTMs) after two-year storage was also investigated to reveal the deactivation mechanism and stabilizing strategy of CuCl carrier [30,42]. As seen from Fig. 7a–b, both DES-FTM and IL-FTM suffered from severe deterioration, and some reddish-brown clusters were uniformly dispersed on the surface of DES-FTM, while the whole surface of IL-FTM was completely covered by fine reddish-brown particles with obvious agglomerations, indicating instability and deactivation of CuCl. In contrast, the Cu-DESM remained green and transparent, which was unchanged in relative to pristine membrane and indicated the excellent stability of Cu-DESM (Fig. 7c). As revealed by Fig. 7d, the surface of DES-FTM exhibited some particle clusters consisted of stone-like

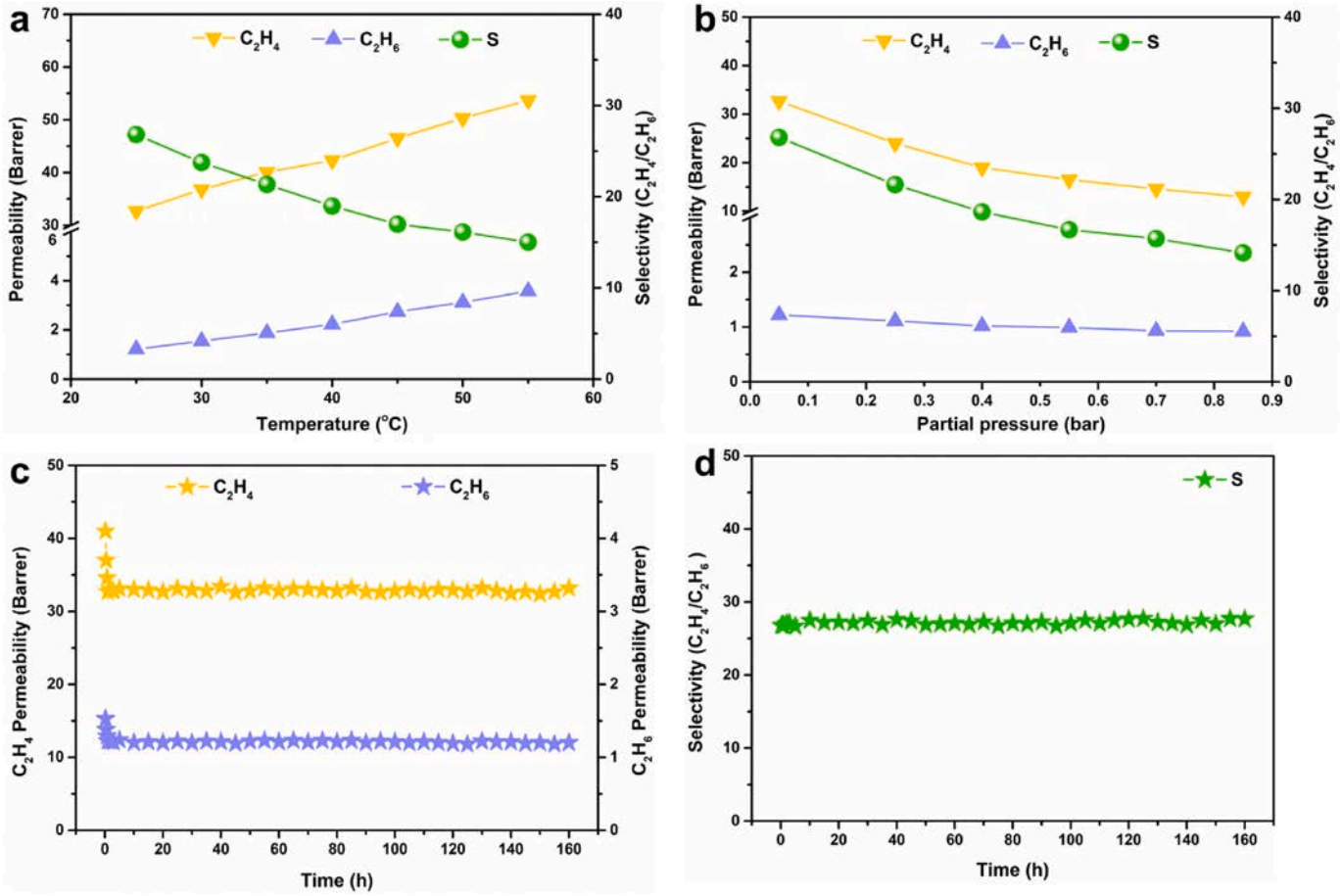

Fig. 6. Optimization of operating conditions and long-term stability of Cu-DESMs, where the [EAHCl][G] based DES is used with the molar ratio of HBA and HBD at 1:2 and CuCl concentration at 3 mol/L. (a) Effect of operating temperature. (b) Effect of partial pressure. (c, d) Long-term stability of Cu-DESMs during continuous 160-h operation. Test conditions: the pressure of 0.1 bar, the temperature of 25 °C and the gas flow rate of 60 mL/min (STP) with equal molar of C_2H_4 and C_2H_6 unless otherwise stated.

particles larger than 10 μm but the membrane pores were still full of CuCl/DES. IL-FTM also had some particle clusters with angular shape and much smaller size, and many pores were empty without any liquid, which suggested the complete destruction of IL-FTM (Fig. 7e). Fortunately, Cu-DESM reported in this work remained the pristine morphology (Fig. 7f). The good chemistry stability of Cu-DESM was further confirmed by ATR-FTIR spectra, no additional peak was detected with the extending of time (Fig. 7g). Therefore, the carrier stability followed the order: Cu-DESM > DES-FTM > IL-FTM, which suggested the DES based membrane possessed better stability due to the encapsulation effect that carriers were solvated and encapsulated by HBD molecules to prevent carrier from moisture and oxygen gas.

The element distribution of DES-FTM, IL-FTM and Cu-DESM as well as crystalline structure were investigated by EDS mapping and XRD patterns. As for DES-FTM (Fig. 7h), the main elements were Cu and Cl and the O content was low, and the XRD curve showed the diffraction peaks of $CuCl_2$, which suggested the carrier deactivation mechanism was dominated by the disproportionated reaction. While IL-FTM was abundant with Cu and O elements (Fig. 7i), and the XRD curve showed the diffraction peaks of basic cupric carbonate, which suggested oxidizing reaction resulted in carrier deactivation. In contrast, Cu-DESM exhibited the unchanged element distribution (Fig. 7j) and XRD pattern with the pristine membrane, which suggested their excellent stability. Compared with DES-FTM and IL-FTM, the good long-term carrier stability of Cu-DESM mainly attributed to the strong hydrogen-bond interactions between HBA and copper complex anion (Fig. 7m) and the encapsulation effect by HBD molecules (Fig. 7l). On the one hand, the HBA possessed Brønsted-acidity and spontaneously generated strong hydrogen-bond interactions with copper complex anion, which not only enhanced carrier activity but also enhanced carrier stability. On the other hand, the copper complex anions were solvated and encapsulated by HBD molecules, which protected carrier from moisture and oxygen gas and thus promoted carrier stability.

3.6. Comparison

Various membranes with different materials and structures had been used in C_2H_4/C_2H_6 separation, including polymers membranes [4,5], CMS membranes [12,51], MMMs [8,52], MOF membranes [14,22], IL membranes [16,28], and DES membranes [31]. The separation performance of the Cu-DESMs prepared in the work were compared to the literature data as well as the Robeson upper bound proposed by Koros [53], and the detailed corresponding data can be found in Tables S2–S7. As demonstrated in Fig. 8, the performances of Cu-DESMs exceeded the upper bound for polymer membranes, and were superior to most of the CMS membranes and MMMs. The Cu-DESMs took the separation performance of copper salt-based FTMs to a new level, and their separation performances were much better than that of previously reported FTMs utilizing copper salt as carrier even with the consideration of the thickness of the membranes (Fig. S6). Although the separation performances of the Cu-DESMs in the work were slightly lower than the performances of silver salt-based FTMs, Cu-DESMs were still very competitive considering the much lower cost of copper salts as well as good stability.

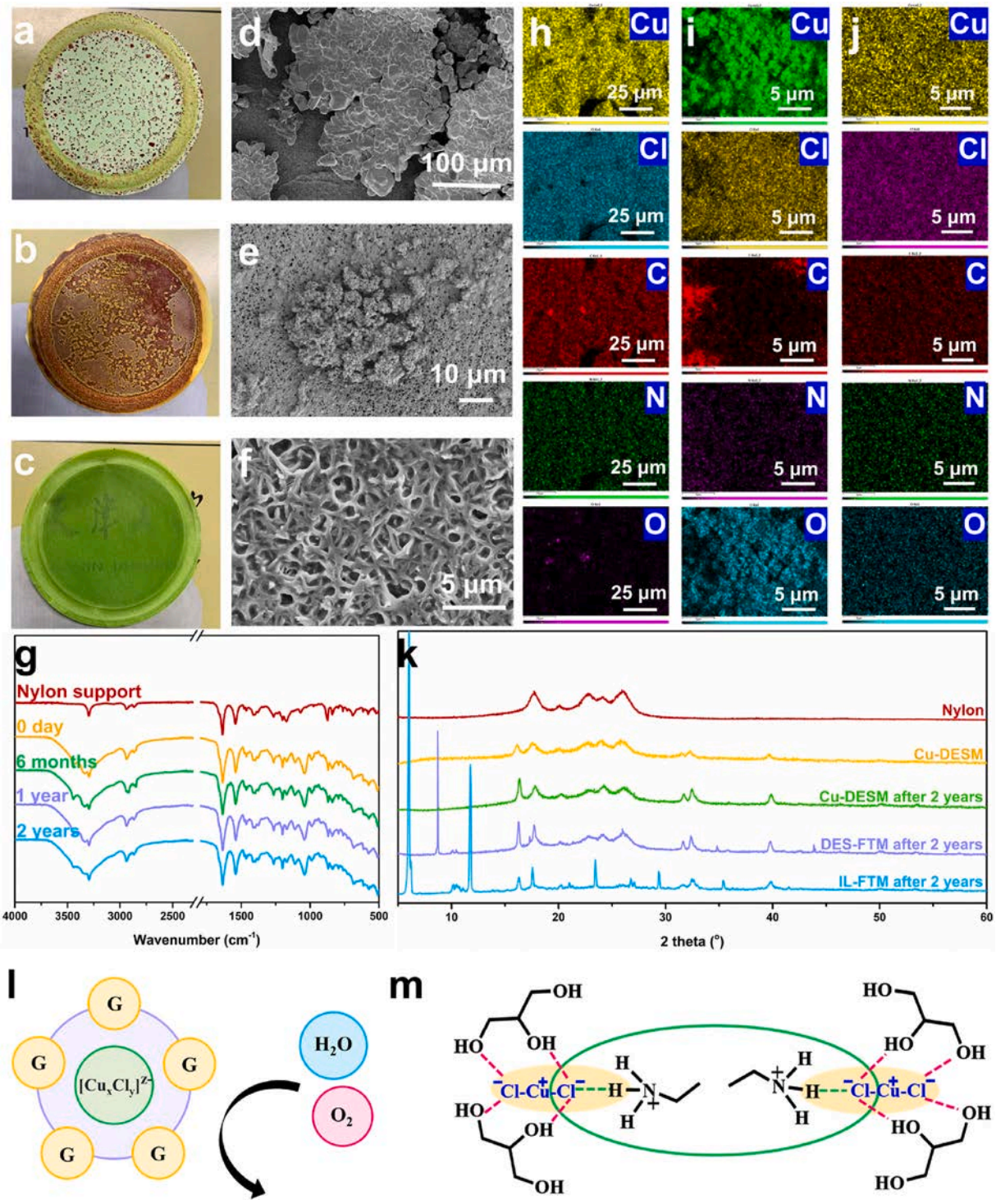

Fig. 7. Comparison of the stability of Cu-DESMs with the previously reported CuCl/IL-FTM and CuCl/DES-FTM to highlight the deactivation mechanism and stabilizing strategy of CuCl carrier, where [EAHCl][G] based DES is used with the molar ratio of HBA and HBD at 1:2 and the CuCl concentration of 3 mol/L (a, b, c) photos of DES-FTM, IL-FTM and Cu-DESM after two-year storage without any protection. (d, h) SEM images and corresponding EDS mapping of DES-FTM. (e, i) SEM images and EDS mapping of IL-FTM. (f,ji) SEM images and EDS mapping of Cu-DESM. (g) FTIR spectra of Cu-DESMs after storage for different times. (k) XRD patterns of DES-FTMs, IL-FTMs, Cu-DESMs after two-year storage. (l) Encapsulation effect by HBD molecules for carrier stability. (m) Hydrogen-bond interactions between $[Cu_xCl_y]^{z-}$ and proton of $-NH_3^+$ for carrier stability.

4. Conclusions

In summary, deactivation mechanism of CuCl carrier such as oxidation and disproportionation reactions in the previously reported membrane was revealed and Brønsted-acidic property was proposed to stabilize CuCl carrier. A series of copper-decorated DES based supported liquid membranes (Cu-DESMs) were constructed by utilizing DESs with Brønsted-acidic property as matrix and CuCl as carrier for highly efficient ethylene/ethane separation, whose successful fabrication was confirmed by SEM and EDS characterizations. The investigation of membrane chemical structure revealed that the complexation reaction between CuCl and Cl^- generated copper complex anions as active

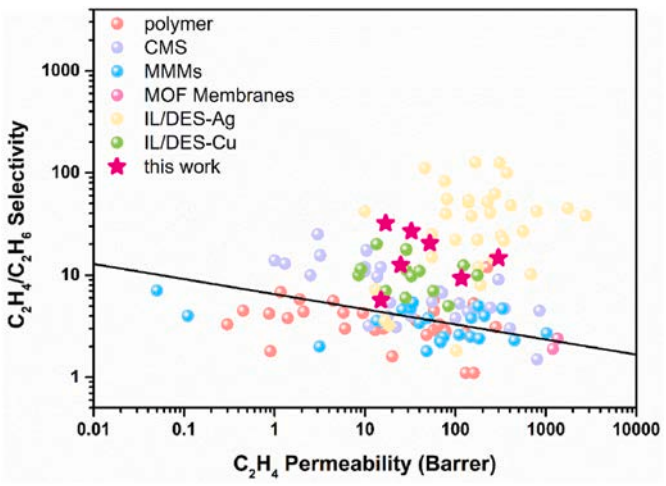

Fig. 8. The comparation of the separation performance of the Cu-DESMs prepared in the work with the-state-of-the-art C_2H_4/C_2H_6 separation membranes in the literatures.

carrier, and the strong hydrogen-bond interactions occurred between protonated cation of HBA or HBD and active carrier. Moreover, the separation performances of Cu-DESMs could be tailored by the molecular design of HBA and HBD, as well as the optimization of HBA/HBD molar ratio and CuCl concentration, which outperformed most of the-state-of-the-art membranes in the literatures. Particularly, Cu-DESMs obtained good stability and was highlighted by comprehensive comparison with the prevalent CuCl based FTMs, which was attributed to the strong hydrogen-bond interactions between HBA and copper complex anion and the encapsulation effect by HBD molecules. This work will arouse more attention for carrier-stability study, and deep insight of carrier deactivation mechanism will shed light on design robust membranes for energy-intensive gas separations.

Author statement

Mi Xu: Conceptualization, Investigation, Data analysis, Validation, Writing–original draft. Haozhen Dou: Data analysis, Writing–review & editing. Feifei Peng, Na Yang, Xiaoming Xiao, Xiaowei Tantai and Yongli Sun: Writing–review & editing. Bin Jiang and Luhong Zhang: Supervision, Funding acquisition.

Declaration of competing interest

The authors declare that they have no known competing financial interests or personal relationships that could have appeared to influence the work reported in this paper.

Acknowledgments

We are grateful for the financial support from National Natural Science Foundation of China (No. 22078233).

Appendix A. Supplementary data

Supplementary data to this article can be found online at https://doi.org/10.1016/j.memsci.2022.120775.

References

[1] Y. Su, S. Cong, M. Shan, Y. Zhang, Enhanced propylene/propane separation in facilitated transport membranes containing multisilver complex, AIChE J. 68 (2022), e17410.
[2] Y. Ren, X. Liang, H. Dou, C. Ye, Z. Guo, J. Wang, Y. Pan, H. Wu, M.D. Guiver, Z. Jiang, Membrane-based olefin/paraffin separations, Adv. Sci. 7 (2020), 2001398.
[3] S. Wang, L. Yang, G. He, B. Shi, Y. Li, H. Wu, R. Zhang, S. Nunes, Z. Jiang, Two-dimensional nanochannel membranes for molecular and ionic separations, Chem. Soc. Rev. 49 (2020) 1071–1089.
[4] W.H. Lee, J.G. Seong, J.Y. Bae, H.H. Wang, Y.M. Lee, Thermally rearranged semi-interpenetrating polymer network (TR-SIPN) membranes for gas and olefin/paraffin separation, J. Membr. Sci. 625 (2021), 119157.
[5] A. Aov, B. Dvg, B. Abya, Development of solid polymer composite membranes based on sulfonated fluorocopolymer for olefin/paraffin separation with high permeability and selectivity, Separ. Purif. Technol. 254 (2021), 117562.
[6] L. Lang, F. Banihashemi, J.B. James, J. Miao, J.Y.S. Lin, Enhancing selectivity of ZIF-8 membranes by short-duration postsynthetic ligand-exchange modification, J. Membr. Sci. 619 (2021), 118743.
[7] T.H. Lee, J.G. Jung, Y.J. Kim, J.S. Roh, H.B. Park, Defect engineering in metal organic frameworks towards advanced mixed matrix membranes for efficient propylene/propane separation, Angew. Chem. Int. Ed. 133 (23) (2021) 13191–13198.
[8] G. Chen, X. Chen, Y. Pan, Y. Ji, W. Jin, M-gallate MOF/6FDA-polyimide mixed-matrix membranes for C_2H_4/C_2H_6 separation, J. Membr. Sci. 620 (2020), 118852.
[9] H. Dou, M. Xu, B. Wang, Z. Zhang, D. Luo, B. Shi, G. Wen, M. Mousavi, A. Yu, Z. Bai, Analogous mixed matrix membranes with self-assembled interface pathways, Angew. Chem. Int. Ed. 60 (2021) 5864–5870.
[10] J.E. Bachman, Z.P. Smith, T. Li, T. Xu, J.R. Long, Enhanced ethylene separation and plasticization resistance in polymer membranes incorporating metal-organic framework nanocrystals, Nat. Mater. 15 (2016) 845–849.
[11] A. Sjk, B. Jfk, A. Yhc, A. Sen, A. Hp, A. Yip, Aging-resistant carbon molecular sieve membrane derived from pre-crosslinked Matrimid for propylene/propane separation, J. Membr. Sci. 636 (2021), 119555.
[12] Q. Wang, F. Huang, C.J. Cornelius, Carbon molecular sieve membranes derived from crosslinkable polyimides for CO_2/CH_4 and C_2H_4/C_2H_6 separations, J. Membr. Sci. 621 (2021), 118785.
[13] Y. Xu, J. Xu, C. Yang, Molecule design of effective C_2H_4/C_2H_6 separation membranes: from 2D nanoporous graphene to 3D AHT zeolite, J. Membr. Sci. 604 (2020), 118033.
[14] J.B. James, J. Wang, L. Meng, Y.S. Lin, ZIF-8 membrane ethylene/ethane transport characteristics in single and binary gas mixtures, Ind. Eng. Chem. Res. 56 (2017) 7567–7575.
[15] R. Deng, Y. Sun, H. Bi, H. Dou, H. Yang, B. Wang, W. Tao, B. Jiang, Deep eutectic solvents as tuning media dissolving Cu^+ used in facilitated transport supported liquid membrane for ethylene/ethane separation, Energy Fuel. 31 (2017) 11146–11155.
[16] M. Xu, B. Jiang, H. Dou, N. Yang, X. Xiao, X. Tantai, Y. Sun, L. Zhang, Customized facilitated transport membranes by mixed strategy for ethylene/ethane separation, Separ. Purif. Technol. 277 (2021), 119484.
[17] L. Yang, H. Yang, H. Wu, L. Zhang, H. Ma, Y. Liu, Y. Wu, Y. Ren, X. Wu, Z. Jiang, COF membranes with uniform and exchangeable facilitated transport carriers for efficient carbon capture, J. Mater. Chem. A. 9 (2021) 12636–12643.
[18] L. Yang, X. Liu, H. Wu, S. Wang, X. Liang, L. Ma, Y. Ren, Y. Wu, Y. Liu, M. Sun, Z. Jiang, Amino-functionalized POSS nanocage intercalated graphene oxide membranes for efficient biogas upgrading, J. Membr. Sci. 596 (2020), 117733.
[19] H. Dou, B. Jiang, M. Xu, Z. Zhang, G. Wen, F. Peng, A. Yu, Z. Bai, Y. Sun, L. Zhang, Boron nitride membranes with a distinct nanoconfinement effect for efficient ethylene/ethane separation, Angew. Chem. Int. Ed. 131 (39) (2019) 14107–14113.
[20] H. Dou, M. Xu, B. Jiang, G. Wen, L. Zhao, B. Wang, A. Yu, Z. Bai, Y. Sun, L. Zhang, Z. Chen, Z. Jiang, Bioinspired graphene oxide membranes with dual transport mechanisms for precise molecular separation, Adv. Funct. Mater. 29 (2019), 1905229.
[21] W. Ying, X. Peng, Graphene oxide nanoslit-confined $AgBF_4$/ionic liquid for efficiently separating olefin from paraffin, Nanotechnology 31 (2019), 085703.
[22] K. Yang, Y. Ban, W. Yang, Layered MOF membranes modified with ionic liquid/$AgBF_4$ composite for olefin/paraffin separation, J. Membr. Sci. 639 (2021), 119771.
[23] Y. Sun, Z. Zhang, L. Tian, H. Huang, C. Geng, X. Guo, Z. Qiao, C. Zhong, Confined ionic liquid-built gas transfer pathways for efficient propylene/propane separation, ACS Appl. Mater. Interfaces 13 (2021) 49050–49057.
[24] W. Zheng, Z. Tian, Z. Wang, D. Peng, Y. Zhang, J. Wang, Y. Zhang, Dual-function biomimetic carrier based facilitated transport mixed matrix membranes with high stability for efficient CO_2/N_2 separation, Separ. Purif. Technol. (2021), 120371.
[25] C.M. Sanchez, T. Song, J.F. Brennecke, B.D. Freeman, Hydrogen stable supported ionic liquid membranes with silver carriers: propylene and propane permeability and solubility, Ind. Eng. Chem. Res. 59 (2020) 5362–5370.
[26] M. Fallanza, A. Ortiz, D. Gorri, I. Ortiz, Polymer-ionic liquid composite membranes for propane/propylene separation by facilitated transport, J. Membr. Sci. 444 (2013) 164–172.
[27] L.C. Tomé, D. Mecerreyes, C.S.R. Freire, L.P.N. Rebelo, I.M. Marrucho, Polymeric ionic liquid membranes containing IL-Ag^+ for ethylene/ethane separation via olefin-facilitated transport, J. Mater. Chem. A. 2 (2014) 5631–5639.
[28] M. Xu, B. Jiang, H. Dou, N. Yang, X. Xiao, X. Tantai, Y. Sun, L. Zhang, Double-salt ionic liquid derived facilitated transport membranes for ethylene/ethane separation, J. Membr. Sci. 639 (2021), 119773.
[29] H. Dou, B. Jiang, X. Xiao, M. Xu, X. Tantai, B. Wang, Y. Sun, L. Zhang, Novel protic ionic liquid composite membranes with fast and selective gas transport nanochannels for ethylene/ethane separation, ACS Appl. Mater. Interfaces 10 (2018) 13963–13974.

[30] B. Jiang, H. Dou, L. Zhang, B. Wang, Y. Sun, H. Yang, Z. Huang, H. Bi, Novel supported liquid membranes based on deep eutectic solvents for olefin-paraffin separation via facilitated transport, J. Membr. Sci. 536 (2017) 123–132.
[31] B. Jiang, J. Zhou, M. Xu, H. Dou, H. Zhang, N. Yang, L. Zhang, Multifunctional ternary deep eutectic solvent-based membranes for the cost-effective ethylene/ethane separation, J. Membr. Sci. 610 (2020), 118243.
[32] T.C. Merkel, R. Blanc, I. Ciobanu, B. Firat, A. Suwarlim, J. Zeid, Silver salt facilitated transport membranes for olefin/paraffin separations: carrier instability and a novel regeneration method, J. Membr. Sci. 447 (2013) 177–189.
[33] A. Campos, R. Reis, A. Ortiz, D. Gorri, I. Ortiz, A perspective of solutions for membrane instabilities in olefin/paraffin separations: a review, Ind. Eng. Chem. Res. 57 (2018) 10071–10085.
[34] M.N. Davenport, C.L. Bentley, J.F. Brennecke, B.D. Freeman, Ethylene and ethane transport properties of hydrogen-stable Ag^{+}-based facilitated transport membranes, J. Membr. Sci. 647 (2022), 120300.
[35] J. Kim, W.K. Sang, S.H. Mun, S.K. Yong, Facile synthesis of copper nanoparticles by ionic liquids and its application to facilitated olefin transport membranes, Ind. Eng. Chem. Res. 48 (2009) 7437–7441.
[36] G.H. Hong, D. Ji, S.W. Kang, Highly permeable ionic liquid/Cu composite membrane for olefin/paraffin separation, Chem. Eng. J. 230 (2013) 111–114.
[37] S. Jeong, S.W. Kang, Effect of Ag_2O nanoparticles on long-term stable polymer/$AgBF_4$/$Al(NO_3)_3$ complex membranes for olefin/paraffin separation, Chem. Eng. J. 327 (2017) 500–504.
[38] H. Dou, B. Jiang, X. Xiao, M. Xu, B. Wang, L. Hao, Y. Sun, L. Zhang, Ultra-stable and cost-efficient protic ionic liquid based facilitated transport membranes for highly selective olefin/paraffin separation, J. Membr. Sci. 557 (2018) 76–86.
[39] H. Dou, B. Jiang, L. Zhang, M. Xu, Y. Sun, Synergy of high permeability, selectivity and good stability properties of silver-decorated deep eutectic solvent based facilitated transport membranes for efficient ethylene/ethane separation, J. Membr. Sci. 567 (2018) 39–48.
[40] H. Dou, M. Xu, B. Wang, Z. Zhang, G. Wen, F. Peng, K. Zarshenas, D. Luo, A. Yu, Z. Bai, Self-assembled facilitated transport membranes with tunable carrier distribution for ethylene/ethane separation, Adv. Funct. Mater. (2021), 2104349.
[41] B. Jiang, W. Tao, H. Dou, Y. Sun, X. Xiao, L. Zhang, N. Yang, A novel supported liquid membrane based on binary metal chloride deep eutectic solvents for ethylene/ethane separation, Ind. Eng. Chem. Res. 56 (51) (2017) 15153–15162.
[42] Y. Sun, H. Bi, H. Dou, H. Yang, Z. Huang, A novel copper(I)-based supported ionic liquid membrane with high permeability for ethylene/ethane separation, Ind. Eng. Chem. Res. 56 (3) (2017) 741–749.
[43] Z. Zhu, H. Lü, M. Zhang, H. Yang, Deep eutectic solvents as non-traditionally multifunctional media for the desulfurization process of fuel oil, Phys. Chem. Chem. Phys. 23 (2) (2021) 785–805.
[44] Y.Y. Lee, D. Penley, A. Klemm, W. Dean, B. Gurkan, Deep eutectic solvent formed by imidazolium cyanopyrrolide and ethylene glycol for reactive CO_2 separations, ACS Sustain. Chem. Eng. 93 (2021) 1090–1098.
[45] X. Liu, B. Wang, X. Lv, Q. Meng, M. Li, Enhanced removal of hydrogen sulfide using novel nanofluid system composed of deep eutectic solvent and Cu nanoparticles, J. Hazard Mater. 405 (2020), 124271.
[46] T. Hanada, M. Goto, Synergistic deep eutectic solvents for lithium extraction, ACS Sustain. Chem. Eng. 9 (2021) 2152–2160.
[47] J.K. Ali, C.M. Chabib, Jaoude M. Abi, Enhanced removal of aqueous phenol with polyimide ultrafiltration membranes embedded with deep eutectic solvent-coated nanosilica, Chem. Eng. J. 408 (2020), 128017.
[48] Y. Zhao, Z. Mai, P. Shen, E. Ortega, J. Shen, C. Gao, B. Van der Bruggen, Nanofiber based organic solvent anion exchange membranes for selective separation of monovalent anions, ACS Appl. Mater. Interfaces 12 (2020) 7539–7547.
[49] G. Michele, K.A. Stevensa, D.R. Paula, B.D. Freemana, Modeling gas permeability and diffusivity in HAB-6FDA polyimide and its thermally rearranged analogs, J. Membr. Sci. 537 (2017) 83–92.
[50] H. Lin, B.D. Freeman, Gas solubility, diffusivity and permeability in poly (ethylene oxide), J. Membr. Sci. 239 (2004) 105–117.
[51] Y.-H. Chu, D. Yancey, L. Xu, M. Martinez, M. Brayden, W. Koros, Iron-containing carbon molecular sieve membranes for advanced olefin/paraffin separations, J. Membr. Sci. 548 (2018) 609–620.
[52] C. Wu, K. Zhang, H. Wang, Y. Fan, T. Li, Enhancing the gas separation selectivity of mixed-matrix membranes using a dual-interfacial engineering approach, J. Am. Chem. Soc. 142 (43) (2020) 18503–18512.
[53] M. Rungta, C. Zhang, W.J. Koros, L. Xu, Membrane-based ethylene/ethane separation: the upper bound and beyond, AIChE J. 59 (2013) 3475–3489.